Ultrahigh Thermal Conductivity of math xmlns="http://www.w3.org/1998/Math/MathML" display="inline">mi>θ/mi>/math>-Phase Tantalum Nitride

Ashis Kundu, Xiaolong Yang, Jinlong Ma, Tianli Feng, Jesús Carrete, Xiulin Ruan, Georg K. H. Madsen, and Wu Li

Phys. Rev. Lett. **126**, 115901 — Published 17 March 2021

DOI: 10.1103/PhysRevLett.126.115901

Ultrahigh thermal conductivity in θ-phase tantalum nitride

Ashis Kundu,[1,2,3] Xiaolong Yang,[1,2] Jinlong Ma,[1,4] Tianli Feng,[5]
Jesús Carrete,[3] Xiulin Ruan,[6] Georg K. H. Madsen,[3] and Wu Li[1,*]

[1] *Institute for Advanced Study, Shenzhen University, Shenzhen 518060, China*
[2] *College of Physics and Optoelectronic Engineering, Shenzhen University, Shenzhen 518060, China*
[3] *Institute of Materials Chemistry, TU Wien, A-1060 Vienna, Austria*
[4] *School of Energy and Power Engineering, Huazhong University of Science and Technology, Wuhan 430074, China*
[5] *Energy and Transportation Science Division, Oak Ridge National Laboratory, Oak Ridge, Tennessee 37831, USA*
[6] *School of Mechanical Engineering and the Birck Nanotechnology Center, Purdue University, West Lafayette, Indiana 47907-2088, USA*

Extracting long-lasting performance from electronic devices and improving their reliability through effective heat management requires good thermal conductors. Taking both three- and four-phonon scattering as well as electron-phonon and isotope scattering into account, we predict that semimetallic θ-phase tantalum nitride (θ-TaN) has an ultrahigh thermal conductivity (κ), of 995 and 822 $\mathrm{W\,m^{-1}\,K^{-1}}$ at room temperature along the a and c axes respectively. Phonons are found to be the main heat carriers, and the high κ hinges on a particular combination of factors: weak electron-phonon scattering, low isotopic mass disorder, and a large frequency gap between acoustic and optical phonon modes that, together with acoustic bunching, impedes three-phonon processes. On the other hand, four-phonon scattering is found to be significant. This study provides new insight into heat conduction in semimetallic solids and extends the search for high-κ materials into the realms of semimetals and non-cubic crystal structures.

Materials with high thermal conductivity are always in demand for thermal management in microelectronic devices [1–3]. Unfortunately, so far only a few systems with thermal conductivities over 1000 $\mathrm{W\,m^{-1}\,K^{-1}}$ at room temperatures have been identified. Diamond, an insulator, is the leader in the category and the best known example, with a room-temperature lattice thermal conductivity ($\kappa_{\mathbf{ph}}$) of around 2000 $\mathrm{W\,m^{-1}\,K^{-1}}$ [4–7]. The semiconductor boron-arsenide (BAs), with a $\kappa_{\mathbf{ph}}$ of $\sim$ 1000-1400 $\mathrm{W\,m^{-1}\,K^{-1}}$ at room temperature [8–11], is a more recent entrant. A way to improve thermal conductivity in a wide range of crystals is to work with isotopically purified samples. This idea has been used to push the room-temperature $\kappa_{\mathbf{ph}}$ of insulator c-BN above the 1000 $\mathrm{W\,m^{-1}\,K^{-1}}$ mark as well, specifically from 850 to 1600 $\mathrm{W\,m^{-1}\,K^{-1}}$ [12]. While the lattice dominates thermal transport in insulators and semiconductors, the heat carriers are predominantly electrons in metals. Metals dominate high-thermal-conductivity materials at low temperatures and high temperatures and can be relatively good thermal conductors at room temperature, with a thermal conductivity as high as 429 $\mathrm{W\,m^{-1}\,K^{-1}}$ for silver [13].

Predicting compounds with a high thermal conductivity is challenging. Most ab-initio studies of $\kappa_{\mathbf{ph}}$ restrict themselves to three-phonon (3ph) and phonon-isotope (ph-iso) scattering. However, as these scattering channels are suppressed, new and unexpected sources become important. The recent discovery of the high thermal conductivity in BAs is an illustrative example of this fact. The prediction was based on an elegant theoretical study taking advantage of As having only one stable isotope and the mass difference between B and As introducing a gap in the phonon spectrum that suppresses 3ph scattering involving two acoustic phonons and an optical phonon (*aao*) [14]. However, because four-phonon (4ph) scattering was neglected [15], the original work strongly overestimated the actual value of the thermal conductivity compared to the experimental findings [8–11]. In addition to 4ph scattering, a metal with a potential high thermal conductivity presents the challenge of phonon-electron (ph-el) scattering further suppressing thermal conductivity [16–18]. As an example, it has been shown how ph-el scattering is responsible for more than half of the scattering in pure W, heavily doped Si and a few transition metal carbides [16, 19–22].

Semimetals are not an obvious place to look for high thermal conductivity compounds: They typically exhibit both a low $\kappa_{\mathbf{ph}}$ and electronic contribution to the thermal conductivity ($\kappa_{\mathbf{e}}$) in the range from a few to a few tens of $\mathrm{W\,m^{-1}\,K^{-1}}$. Graphite is an exception. The in-plane thermal conductivity of graphite can reach around 2000 $\mathrm{W\,m^{-1}\,K^{-1}}$, however, the cross-plane value is less than 10 $\mathrm{W\,m^{-1}\,K^{-1}}$. Semimetallic tungsten carbide (WC) is also known to display an unusually high thermal conductivity at room temperature ($\kappa > 100$ $\mathrm{W\,m^{-1}\,K^{-1}}$)[23], which we recently attributed to an anomalously high $\kappa_{\mathbf{ph}}$ [22]. The results leave the door open to the possibility of finding semimetals with an ultrahigh κ. Among the potential candidates, the θ-phase of tantalum nitride (θ-TaN) has several unique features that make it highly interesting in this respect. First of all, it is isostructural to WC (space group $P\bar{6}m2$; No. 187) and has a similar mass ratio, which could point to low phonon-phonon scattering. Furthermore, the isotope distribution of Ta, the element dominating the heat carrying acoustic vibra-

tional modes, contains almost solely the $^{181}_{74}$Ta nuclide (at a $\sim 99.988\%$ ratio). Finally, the $d-d$ bonding, which is responsible for the semimetallic electronic structure [24], should be stronger than in WC, resulting in a lower density of states (DOS) at the Fermi level and a weaker ph-el coupling. In view of these promising hints, here we use first-principles calculations, taking 3ph, 4ph, ph-iso and ph-el scattering into account, to predict a room-temperature $\kappa_{\mathbf{ph}}$ in the $800-1000\ \mathrm{W\,m^{-1}\,K^{-1}}$ range in semimetallic tantalum nitride (TaN).

Detailed analysis of the results confirms that the high value of $\kappa_{\mathbf{ph}}$ in TaN is indeed only possible thanks to a very special combination of phonon dispersion, a depressed phonon-electron interaction and the virtually non-existing mass-disorder scattering due to the singular isotopic distribution of Ta. Only the low intensity of all scattering mechanisms enables TaN to emerge as such a good thermal conductor.

Methodology.— The lattice thermal conductivity tensor ($\kappa^{\alpha\beta}_{\mathbf{ph}}$) can be calculated in the framework of the linearized Boltzmann transport equation (BTE) using the expression [25]

$$\kappa^{\alpha\beta}_{\mathbf{ph}} = \frac{1}{8\pi^3}\int_{\mathrm{BZ}}\sum_{p} C_V\left(p\mathbf{q}\right) v^{\alpha}_{p\mathbf{q}} F^{\beta}_{p\mathbf{q}} d^3\mathbf{q}, \tag{1}$$

where p runs over all phonon branches, BZ denotes the Brillouin zone of the crystal, α and β are Cartesian axes, and $\omega_{p\mathbf{q}}$, $v^{\alpha}_{p\mathbf{q}}$, $C_V\left(p\mathbf{q}\right)$ and $F^{\beta}_{p\mathbf{q}}$ are the angular frequency, group velocity, contribution to the isobaric heat capacity and mean free displacement, respectively, of phonons from branch p with wave vector $\mathbf{q}$.

Key to determining $\kappa_{\mathbf{ph}}$ are the different phonon scattering mechanisms, which are incorporated into the expression above through $F^{\beta}_{p\mathbf{q}}$. We use the general form of the linearized BTE for phonons [25]:

$$F^{\beta}_{p\mathbf{q}} = \tau_{p\mathbf{q}}\left(v^{\beta}_{p\mathbf{q}} + \Delta^{\beta}_{p\mathbf{q}}\right). \tag{2}$$

Here, $\tau_{p\mathbf{q}}$ is the phonon lifetime, while the $\Delta^{\beta}_{p\mathbf{q}}$ terms depend linearly on $F^{\beta}_{p\mathbf{q}}$ and describe the departure from the relaxation-time approximation (RTA). We obtain $F^{\beta}_{p\mathbf{q}}$ iteratively starting from the RTA [25, 26].

The inverse of $\tau_{p\mathbf{q}}$ is the scattering rate and is expressed as a sum of the contributions from the different scattering mechanisms. We exhaustively explore all plausible contributions to avoid overestimating the thermal conductivity. Specifically, we include three-phonon (3ph), four-phonon (4ph) phonon-isotope (ph-iso) and phonon-electron (ph-el) scattering in our calculations.

$$\frac{1}{\tau_{p\mathbf{q}}} = \frac{1}{\tau^{\mathrm{3ph}}_{p\mathbf{q}}} + \frac{1}{\tau^{\mathrm{4ph}}_{p\mathbf{q}}} + \frac{1}{\tau^{\mathrm{ph\text{-}iso}}_{p\mathbf{q}}} + \frac{1}{\tau^{\mathrm{ph\text{-}el}}_{p\mathbf{q}}}. \tag{3}$$

Phonon-electron scattering involves only one phonon and does not affect $\Delta^{\beta}_{p\mathbf{q}}$ [19]. Furthermore, four-phonon scattering is dominated by Umklapp processes[15, 27] and their contribution to $\Delta^{\beta}_{p\mathbf{q}}$ can be neglected. The detailed expressions for $\Delta_{p\mathbf{q}}$, $1/\tau^{\mathrm{ph\text{-}iso}}_{p\mathbf{q}}$, $1/\tau^{\mathrm{3ph}}_{p\mathbf{q}}$, $1/\tau^{\mathrm{4ph}}_{p\mathbf{q}}$, $1/\tau^{\mathrm{ph\text{-}el}}_{p\mathbf{q}}$ can be found in Refs. 16, 19, 25–29.

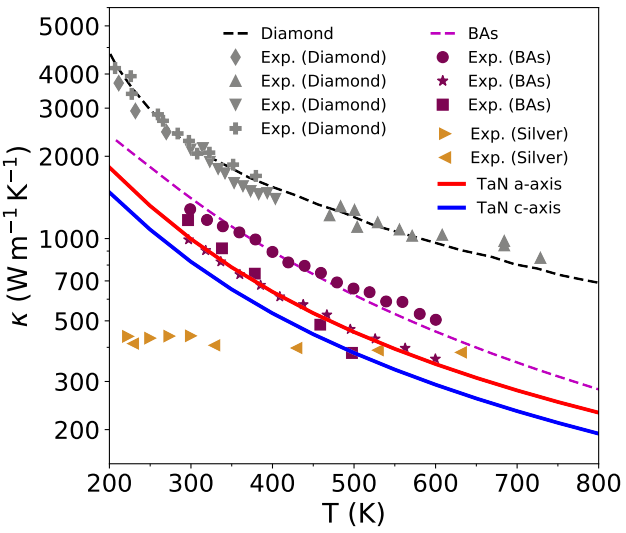

FIG. 1. Calculated total thermal conductivity ($\kappa = \kappa_{\mathrm{e}} + \kappa_{\mathrm{ph}}$) as a function of temperature for TaN along the a and c axes in comparison with available results of κ for diamond and BAs. Theoretical results for diamond and BAs are taken from Ref. 14 and 27. Experimental results for diamond (rhomboids [4], upward-pointing triangles [6], downward-pointing triangles [5] and plus signs [7]), BAs (circles [10], squares [9], and stars [8]) and silver (right-pointing triangles [36], left-pointing triangles [37]) are also shown.

The main inputs needed to solve the phonon BTE are harmonic and anharmonic interatomic force constants (IFCs). All the IFCs and the details of the electronic structure, are extracted from density functional theory calculations carried out using the projector-augmented plane wave method [30] as implemented in VASP [31, 32]. For the calculation of phonon-electron scattering elements, the EPW software [33], based on maximally localized Wannier functions is used along with the QUANTUM ESPRESSO package [34]. Finally, the ShengBTE package [25], modified to include the phonon-electron and four-phonon scattering rates, is employed to calculate $\kappa_{\mathbf{ph}}$. Further computational details are given in the Supplementary Material [35].

Figure 1 shows the calculated total thermal conductivity (κ) of TaN as a function of temperature. Its values at 300 K are 995 and 820 $\mathrm{W\,m^{-1}\,K^{-1}}$ along the a and c axes respectively. The electronic contributions to the thermal conductivity ($\kappa_{\mathbf{e}}$) are 36 and 18 $\mathrm{W\,m^{-1}\,K^{-1}}$, respectively (see Supplementary Material [35]). In contrast, at the same temperature the lattice contributions are around twenty-seven times as much, namely 959 and 802 $\mathrm{W\,m^{-1}\,K^{-1}}$, respectively. This unusually high value of the thermal conductivity, close to the 1000 $\mathrm{W\,m^{-1}\,K^{-1}}$ mark, is the second largest ever predicted for a metallic

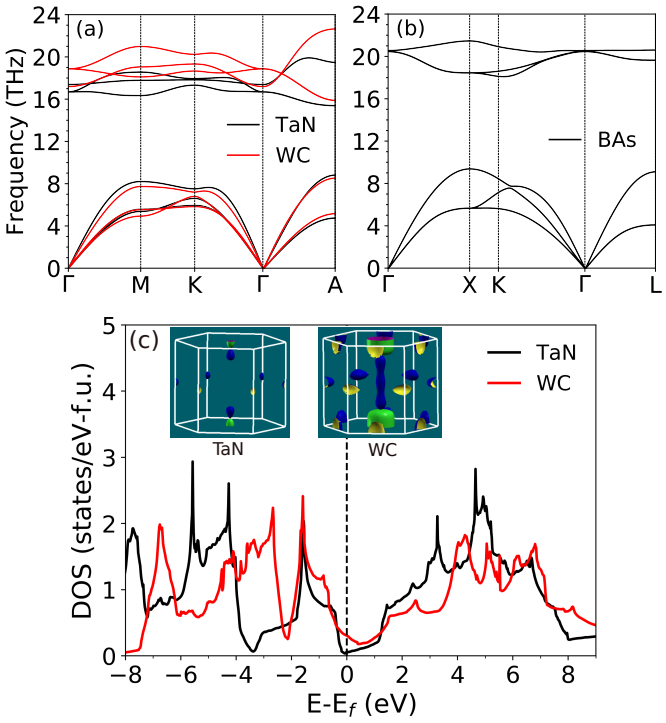

FIG. 2. Calculated phonon dispersion along high-symmetry directions for (a) TaN and WC and (b) BAs. (c) Calculated electronic DOS for TaN and WC. E_f denotes the Fermi energy. The insets show the bulk Fermi surfaces for both compounds.

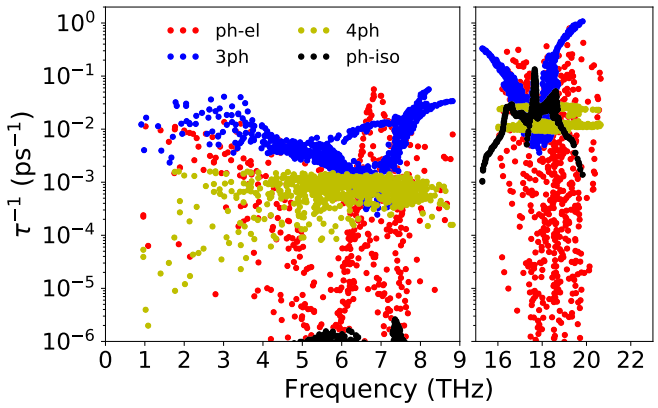

FIG. 3. Calculated three-phonon (3ph), four-phonon (4ph), phonon-isotope (ph-iso), and phonon-electron (ph-el) scattering rates for TaN at 300 K.

system following graphite, more than 100% higher than that of silver and seven times as much as the value for semimetallic WC. In contrast, the calculated electrical conductivity of TaN is one order-of-magnitude higher than graphite (the in-plane directions), one order-of-magnitude smaller than silver and comparable to WC (see Supplementary Material [35]). However, the κ, mostly contributed by phonons, puts TaN in the same range as BAs and diamond. The temperature dependence of the thermal conductivity of TaN is also very similar to the case of BAs, and in particular falls faster than that of diamond above room temperature. The exceptionally high values of $\kappa_{\mathbf{ph}}$ have their origin in stiff interatomic bonding, low electronic DOS in the relevant energy ranges, and low mass disorder due to the limited spread of the natural isotopic mixture of the constituent elements. We explain each of these elements in the following.

The lattice contribution to thermal transport is strongly dependent on the features of the phonon dispersions. As shown in Fig. 2, TaN is similar to BAs from a vibrational point of view in that both have a significant gap between the acoustic and optical branches. Moreover, both compounds exhibit bunching in the acoustic region. These features result in weak 3ph scattering, especially at intermediate frequencies and can lead to a gamut of anomalous phonon transport behaviors, including large values of $\kappa_{\mathbf{ph}}$, marked isotope effects, and a weak temperature dependence of $\kappa_{\mathbf{ph}}$ [14, 21, 22, 38]. The large frequency gap between acoustic and optical phonon modes impedes *aao* 3ph scattering processes. A second class of processes, *aoo*, with two optical phonons involved, is limited to a narrow region of low-frequency acoustic phonons because of the low optical bandwidth of TaN. Finally, the bunching of the acoustic branches constrains the phase space for 3ph processes even further by limiting *aaa* processes with three acoustic phonons. Together, all these restrictions lead to a very weak 3ph contribution to the scattering rates, which plays a major role in the high thermal conductivity of TaN.

In addition to those relationships between the frequency ranges of different phonon branches, the magnitude of the phonon frequencies is also an important indicator. In this case, despite Ta being a much heavier element than B or As, the vibrational frequencies of TaN are in the same range as those of BAs. This suggests that the interatomic bonding in TaN is also much stiffer. That rigidity hints at shorter thermal displacements of the atoms that can make the system less anharmonic than it would otherwise be and reduce the intensity of n-phonon scattering even further.

Figure 3 shows the phonon scattering rates. Due to the features described in the preceding paragraph, including the acoustic-optical gap and acoustic bunching, the 3ph scattering rates have a very marked dip around 7 THz. By way of reference, the 3ph scattering rates of TaN are less than half as much as those of Si [16], and only slightly higher than those of BAs [15, 27]. The latter point is interesting because bonding, considered alone, would suggest lower scattering rates. However, the intrinsic anharmonicity of the potential energy landscape, as characterized by the Grüneisen parameter, is much stronger (1.44 for TaN vs. 0.76 for BAs).

Weak 3ph scattering is not enough to guarantee a very high $\kappa_{\mathbf{ph}}$, a point illustrated by the counterexample of WC. As shown in Fig. 2, that compound has a very similar phonon dispersion as TaN, especially in the acoustic range, where the heavy atom exerts a dominant influence. The slightly lower optical phonon frequencies in TaN are due to the heavier mass of N compared to C, since TaN and WC also have the same number of valence electrons and thus similar bonding properties. In fact, the 3ph scattering rates of WC are also in the same order as those of TaN [22]. However, though the $\kappa_{\mathbf{ph}}$ of WC is much larger than those of other metallic systems, it is still seven times lower than TaN. The explanation lies in the important role found to be played by ph-el scattering in WC, which also leaves a trace in the weak temperature dependence of κ. In contrast, as shown in Fig. 3, ph-el scattering is only dominant for a very limited subset of phonon modes in TaN. To put this in more quantitative terms, neglecting electron scattering would increase the component of $\kappa_{\mathbf{ph}}$ along the a axis by 18% at 300 K, from 959 to 1136 (see Fig. 4). The same thought experiment on WC would lead to a corresponding increment of 230%.

It is the direct $d-d$ bonding between the metal atoms which is responsible for the WC structure type being semimetallic, i.e. close to exhibiting a electronic band gap [24]. The Ta d-orbitals, feeling a smaller effective nuclear charge, should be more extended than those of W. We would thus expect the $d-d$ bonding to be stronger and hence the semiconducting character to be slightly more pronounced in TaN. As shown in Fig. 2, the electronic DOS at the Fermi level and the Fermi surface area is indeed smaller in TaN compared to WC. The intensity of ph-el scattering is known to be positively correlated with the electronic DOS at the Fermi level [18, 20, 22, 39]. Considering this link between the bonding and the weak ph-el scattering, we have analyzed the DOS of a number of transition metal carbides and nitrides, see Supplementary Material [35]. We find that most have a high DOS at the Fermi level. Among the very few that do not, only TaN also fulfills the conditions of a large acoustic-optical gap and low isotopic mass disorder. In this regard, TaN is unique from other transition metal carbides and nitrides and probably the only one of them meeting the requirements for an ultrahigh $\kappa_{\mathbf{ph}}$.

As mentioned in the introduction, mass-disorder scattering due to the natural distribution of isotopes in the constituent elements makes a determinant, easily measurable contribution to $\kappa_{\mathbf{ph}}$ in most materials, to the point that isotopically purified samples can have a significantly higher thermal conductivity than their unenriched counterparts. This is not, however, the case of TaN, where isotope scattering is almost four orders of magnitude less intense than ph-ph scattering. As a result, complete isotopic enrichment of TaN would only lead to an increase of around 2% in $\kappa_{\mathbf{ph}}$ (see Fig. 4), whereas a similar process would increase the $\kappa_{\mathbf{ph}}$ of BAs [15] by a much larger 19%. As already discussed, the dominant contribution to $\kappa_{\mathbf{ph}}$ comes from the acoustic phonons, corresponding to vibrations dominated by the heavier atom. While tantalum is not strictly monoisotopic like arsenic, it can still be considered technically so, as the second isotope contains an exceptionally long-lived but extremely rare metastable state of the $^{180}_{74}$Ta nuclide and is only present at a tiny concentration of 0.012% in natural samples. Therefore, mass-disorder scattering is introduced exclusively by the lighter atom in both TaN and BAs. The smaller spread of the isotopic distribution of N with respect to that of B thus leads to weaker phonon-isotope scattering in TaN.

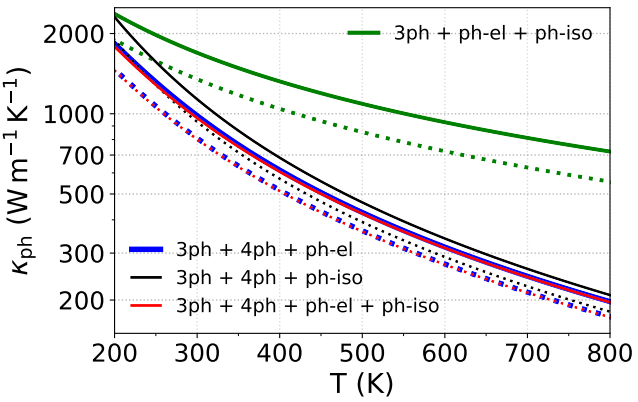

FIG. 4. Temperature dependence of κ_{ph} in TaN when only certain combinations of phonon scattering mechanisms are considered. The solid and dotted lines correspond to the $\kappa_{\mathbf{ph}}$ along the a and c axes, respectively.

Given the constraints that the conservation of energy imposes on 3ph scattering, processes involving four phonons play a vital role, just like in BAs [8–10, 27, 29]. The large acoustic-optical gap forbids the combination of two acoustic phonons into an optical phonon (aao), but combination of acoustic phonons into optical phonons can still occur through 4ph processes [15, 27, 29]. As a result, 4ph scattering dominates over the three-phonon scattering rates at intermediate frequencies around 7 THz, where the scattering rates due to the latter are very weak. Accordingly, 4ph processes account for a $\sim 43\%$ reduction of $\kappa_{\mathbf{ph}}$ at room temperature, an even more marked difference than in BAs, where the difference is 36%. The impact of four-phonon scattering is also felt in the temperature dependence of the thermal conductivity, whose fall is steeper in TaN and BAs than in diamond. In fact, historically BAs had initially been predicted to show a less marked T dependence than diamond before 4ph processes were included in the calculation.

Finally, to illustrate which frequency ranges are affected by the different scattering mechanisms, in Fig. 5 we plot the spectral contribution to $\kappa_{\mathbf{ph}}$ from phonons in

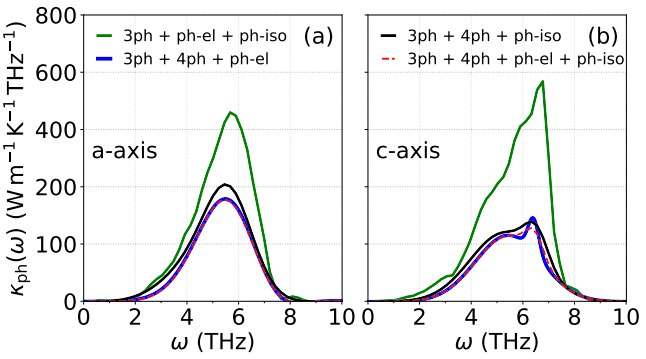

FIG. 5. Calculated spectral contributions to the $\kappa_{\mathbf{ph}}$ at 300 K along the a axis (a) and along the c axis (b), when only particular subsets of phonon scattering mechanisms are taken into account.

each frequency interval when only certain combinations of phonon-phonon (3ph and 4ph), ph-iso, and ph-el interactions are considered as limiting factors. The main contribution to the total $\kappa_{\mathbf{ph}}$ comes from frequencies between 4 and 7 THz. This is a direct manifestation of the effect of the bunching of the acoustic branches, whereby 3ph scattering rates are weakened.

In summary, we predict an ultrahigh κ in semimetallic WC-type TaN using a first-principles approach based on the BTE and exhaustively considering all plausible relevant contributions to heat carrier scattering. The room-temperature thermal conductivity values obtained for this compound are close to the 1000 W m^{-1} K^{-1} mark, 995 and 820 W m^{-1} K^{-1} along the a and c axes, respectively. This unusually high value of the thermal conductivity is the more than double that of silver and the largest ever predicted for a metallic system. Interestingly, the lattice contribution to thermal transport is around twenty-seven times larger than that from electrons, and thus almost single-handedly determines the value of κ.

The high value of $\kappa_{\mathbf{ph}}$ in TaN is only possible thanks to a unique combination of phononic, electronic and even nuclear properties. On top of the presence of a large acoustic-optical gap and a significant degree of bunching of the acoustic branches, the singular isotopic distribution of Ta leads to very weak mass-disorder scattering and the low electronic DOS at the Fermi level to depressed phonon-electron interactions. In light of those requirements, our exploration of 4d and 5d transition metal carbides and nitrides shows that TaN is the only compound in this family likely to have an ultrahigh $\kappa_{\mathbf{ph}}$.

A final remarkable feature is that the phase of TaN studied in this work has a simple hexagonal structure, as opposed the previously known cubic diamond, BAs and c-BN high thermal conductivity compounds. There exist other phases of TaN also, such as ϵ-TaN (CoSn structure type) and δ-TaN (NaCl structure type) [40]. However, the $\kappa_{\mathbf{ph}}$ of those phases can be safely predicted to be lower than the results presented here (see Supplementary Material [35]). In addition to the potential thermal management application, applications that require both high thermal and high electrical conductivities such as leadframes [41] and diffusion barriers in integrated circuits [42] could represent compelling cases for TaN. Besides understanding the factors behind the ultrahigh κ in TaN, we expect this study to guide and motivate the search for further good thermal conductors in the landscape of metallic and semimetallic materials with non-cubic structures.

The authors acknowledge support from the Natural Science Foundation of China (NSFC) under Grant No. 11704258, the Shenzhen Science, Technology and Innovation Commission under Grant No. JCYJ20170412105922384, and the Austrian Science Funds (FWF) under project CODIS (Grant No. FWF-I-3576-N36). J.M. also acknowledges support from NSFC under Grant No.11804229. X.Y. also acknowledges support from the NSFC under Grant No. 12004254.

* wu.li.phys2011@gmail.com

[1] P. Ball, Nature News **492**, 174 (2012).
[2] S. V. Garimella, L.-T. Yeh, and T. Persoons, IEEE Transactions on Components, Packaging and Manufacturing Technology **2**, 1307 (2012).
[3] M. M. Waldrop, Nature News **530**, 144 (2016).
[4] R. Berman, P. R. W. Hudson, and M. Martinez, J. Phys. C: Solid State Phys. **8**, L430 (1975).
[5] D. G. Onn, A. Witek, Y. Z. Qiu, T. R. Anthony, and W. F. Banholzer, Phys. Rev. Lett. **68**, 2806 (1992).
[6] J. R. Olson, R. O. Pohl, J. W. Vandersande, A. Zoltan, T. R. Anthony, and W. F. Banholzer, Phys. Rev. B **47**, 14850 (1993).
[7] L. Wei, P. K. Kuo, R. L. Thomas, T. R. Anthony, and W. F. Banholzer, Phys. Rev. Lett. **70**, 3764 (1993).
[8] F. Tian, B. Song, X. Chen, N. K. Ravichandran, Y. Lv, K. Chen, S. Sullivan, J. Kim, Y. Zhou, T.-H. Liu, M. Goni, Z. Ding, J. Sun, G. A. G. Udalamatta Gamage, H. Sun, H. Ziyaee, S. Huyan, L. Deng, J. Zhou, A. J. Schmidt, S. Chen, C.-W. Chu, P. Y. Huang, D. Broido, L. Shi, G. Chen, and Z. Ren, Science **361**, 582 (2018).
[9] S. Li, Q. Zheng, Y. Lv, X. Liu, X. Wang, P. Y. Huang, D. G. Cahill, and B. Lv, Science **361**, 579 (2018).
[10] J. S. Kang, M. Li, H. Wu, H. Nguyen, and Y. Hu, Science **361**, 575 (2018).
[11] C. Dames, Science **361**, 549 (2018).
[12] K. Chen, B. Song, N. K. Ravichandran, Q. Zheng, X. Chen, H. Lee, H. Sun, S. Li, G. A. G. Udalamatta Gamage, F. Tian, Z. Ding, Q. Song, A. Rai, H. Wu, P. Koirala, A. J. Schmidt, K. Watanabe, B. Lv, Z. Ren, L. Shi, D. G. Cahill, T. Taniguchi, D. Broido, and G. Chen, Science **367**, 555 (2020).
[13] C. Kittel, *Introduction to Solid State Physics, 6th ed.* (John Wiley & Sons, New York, 1986) p. 402.
[14] L. Lindsay, D. A. Broido, and T. L. Reinecke, Phys. Rev.

Lett. **111**, 025901 (2013).
[15] X. Yang, T. Feng, J. Li, and X. Ruan, Phys. Rev. B **100**, 245203 (2019).
[16] B. Liao, B. Qiu, J. Zhou, S. Huberman, K. Esfarjani, and G. Chen, Phys. Rev. Lett. **114**, 115901 (2015).
[17] A. Jain and A. J. H. McGaughey, Phys. Rev. B **93**, 081206 (2016).
[18] Y. Wang, Z. Lu, and X. Ruan, J. Appl. Phys. **119**, 225109 (2016).
[19] Y. Chen, J. Ma, and W. Li, Phys. Rev. B **99**, 020305 (2019).
[20] B. Dongre, J. Carrete, S. Wen, J. Ma, W. Li, N. Mingo, and G. K. H. Madsen, J. Mater. Chem. A **8**, 1273 (2020).
[21] C. Li, N. K. Ravichandran, L. Lindsay, and D. Broido, Phys. Rev. Lett. **121**, 175901 (2018).
[22] A. Kundu, J. Ma, J. Carrete, G. K. H. Madsen, and W. Li, Mater. Today Phys. **13**, 100214 (2020).
[23] A. Gubernat, P. Rutkowski, G. Grabowski, and D. Zientara, International Journal of Refractory Metals and Hard Materials **43**, 193 (2014).
[24] S. D. Wijeyesekera and R. Hoffmann, Organometallics **3**, 949 (1984).
[25] W. Li, J. Carrete, N. A. Katcho, and N. Mingo, Comput. Phys. Commun. **185**, 1747 (2014).
[26] W. Li, Phys. Rev. B **92**, 075405 (2015).
[27] T. Feng, L. Lindsay, and X. Ruan, Phys. Rev. B **96**, 161201 (2017).
[28] A. Ward, D. A. Broido, D. A. Stewart, and G. Deinzer, Phys. Rev. B **80**, 125203 (2009).
[29] T. Feng and X. Ruan, Phys. Rev. B **93**, 045202 (2016).
[30] P. E. Blöchl, Phys. Rev. B **50**, 17953 (1994).
[31] G. Kresse and J. Furthmüller, Phys. Rev. B **54**, 11169 (1996).
[32] G. Kresse and D. Joubert, Phys. Rev. B **59**, 1758 (1999).
[33] S. Ponc, E. Margine, C. Verdi, and F. Giustino, Comput. Phys. Commun. **209**, 116 (2016).
[34] P. Giannozzi, S. Baroni, N. Bonini, M. Calandra, R. Car, C. Cavazzoni, D. Ceresoli, G. L. Chiarotti, M. Cococcioni, I. Dabo, A. D. Corso, S. de Gironcoli, S. Fabris, G. Fratesi, R. Gebauer, U. Gerstmann, C. Gougoussis, A. Kokalj, M. Lazzeri, L. Martin-Samos, N. Marzari, F. Mauri, R. Mazzarello, S. Paolini, A. Pasquarello, L. Paulatto, C. Sbraccia, S. Scandolo, G. Sclauzero, A. P. Seitsonen, A. Smogunov, P. Umari, and R. M. Wentzcovitch, J. Phys. Condens. Matter **21**, 395502 (2009).
[35] See Supplementary Material at "link" for detailed information regarding computational details, convergence test of $\kappa_{\mathbf{ph}}$ with respect to the cut-off for third-order IFCs and $\mathbf{q}$ grids, electronic thermal conductivity, density of states for transition metal carbides and nitrides, lattice thermal conductivity of other phases of TaN and the importance of accurate solution of the Boltzmann transport equation (BTE) for TaN, which includes Refs.[43–52].
[36] Z. Cheng, L. Liu, S. Xu, M. Lu, and X. Wang, Sci. Rep. **5**, 10718 (2015).
[37] Y. S. Touloukian, R. W. Powell, C. Y. Ho, and P. G. Klemens, *Thermal Conductivity: Metallic Elements and Alloys*, Thermophysical Prosperties of Matter 1 (Ifi/Plenum, New York, Washington, 1970).
[38] L. Lindsay, D. A. Broido, J. Carrete, N. Mingo, and T. L. Reinecke, Phys. Rev. B **91**, 121202 (2015).
[39] B. Xu and M. J. Verstraete, Phys. Rev. Lett. **112**, 196603 (2014).
[40] A. Friedrich, W. Morgenroth, L. Bayarjargal, E. A. Juarez-Arellano, B. Winkler, and Z. Konpkov, High Pressure Research **33**, 633 (2013).
[41] S. Krishnan, S. Wang, and M. R. Muhamad, in *2006 Thirty-First IEEE/CPMT International Electronics Manufacturing Technology Symposium* (2006) pp. 236–247.
[42] W.-L. Wang, C.-T. Wang, W.-C. Chen, K.-T. Peng, M.-H. Yeh, H.-C. Kuo, H.-J. Chien, J.-C. Chuang, and T.-H. Ying, Journal of Nanomaterials **2015**, 9 (2015).
[43] A. Friedrich, B. Winkler, L. Bayarjargal, E. A. Juarez Arellano, W. Morgenroth, J. Biehler, F. Schrder, J. Yan, and S. M. Clark, Journal of Alloys and Compounds **502**, 5 (2010).
[44] H. Weng, C. Fang, Z. Fang, and X. Dai, Phys. Rev. B **93**, 241202 (2016).
[45] J. B. He, D. Chen, W. L. Zhu, S. Zhang, L. X. Zhao, Z. A. Ren, and G. F. Chen, Phys. Rev. B **95**, 195165 (2017).
[46] A. Togo and I. Tanaka, Scripta Materialia **108**, 1 (2015).
[47] N. Troullier and J. L. Martins, Phys. Rev. B **43**, 1993 (1991).
[48] W. Li, N. Mingo, L. Lindsay, D. A. Broido, D. A. Stewart, and N. A. Katcho, Phys. Rev. B **85**, 195436 (2012).
[49] W. Li, L. Lindsay, D. A. Broido, D. A. Stewart, and N. Mingo, Phys. Rev. B **86**, 174307 (2012).
[50] E. I. Isaev, S. I. Simak, I. A. Abrikosov, R. Ahuja, Y. K. Vekilov, M. I. Katsnelson, A. I. Lichtenstein, and B. Johansson, J. Appl. Phys. **101**, 123519 (2007).
[51] S.-D. Guo and B.-G. Liu, Journal of Physics: Condensed Matter **30**, 105701 (2018).
[52] S.-D. Guo and P. Chen, J. Chem. Phys. **148**, 144706 (2018).